Journal of The Electrochemical Society, **155** (10) E131-E135 (2008)
0013-4651/2008/155(10)/E131/5/$23.00 © The Electrochemical Society

Electrochemical Approach for Selenization of Stacked Cu–In Layers for Formation of Crystalline $CuInSe_2$

T. P. Gujar,[a,z] V. R. Shinde,[a] Jong-Won Park,[a,b] Hyun Kyung Lee,[b] Kwang-Deog Jung,[a] and Oh-Shim Joo[a,z]

[a]*Clean Energy Research Center, Korea Institute of Science and Technology, Seoul 130-650, Korea*
[b]*The Industrial Chemistry, University of Sang-Myung, Seoul 130-650, Korea*

We report an electrochemical approach to form crystalline $CuInSe_2$ (CIS) films onto indium-tin-oxide substrates via thermal treatment to Se-coated Cu–In alloy. The simultaneous deposition of Cu–In alloy with optimum thickness was obtained by an electrochemical method from a mixture of aqueous solutions of $CuSO_4$ and $In_2(SO_4)_3$ at constant potential. Further, the electrochemical method was used for deposition of elemental Se onto the priorly deposited Cu–In alloy film. To produce CIS films, Se-coated Cu–In alloy films were annealed in argon atmosphere at different temperatures ca. 350–450°C for 30 min. The Cu–In alloy, Se-coated Cu–In alloy, and thermally treated films were characterized using X-ray diffraction to identify the phases and scanning electron microscopy to observe the surface morphology.
 [DOI: 10.1149/1.2957923]

Manuscript submitted April 3, 2008; revised manuscript received June 18, 2008. Published July 29, 2008.

It is well known that photovoltaic devices based on $CuInGaSe_2$ (CIGS) films by sequential coevaporation have reached an efficiency up to 19.9% over small areas of around 0.5 cm^2.[1] However, the use of this technique has limitations for commercial utilization of the solar cells due to the problems associated with large-area uniformity.[2] Alternatively, several other techniques have been used for the growth of CIGS and $CuInSe_2$ (CIS) films such as metall-organic vapor phase[3] and molecular beam epitaxy,[4] chemical bath deposition,[5] successive ionic layer adsorption and reaction,[6] electrodeposition,[7] etc. Because industrial applications need low-cost processing methods for the large-scale production of materials with necessary performance, efforts to find alternative methods are still in progress. One such method, which is simple, low-cost, and applicable for large-scale production, is electrodeposition. The electrochemical methods to form CIS consist of either formation of stacking layers (i.e., CuSe and InSe) and subsequent conversion to CIS by annealing treatments or deposition of CIS from a single bath, followed by thermal annealing in H_2Se or elemental Se atmosphere or etching process.[8-20] Most papers reflect that the as-deposited CIS film is either amorphous or has weak reflections of chalcopyrite CIS, otherwise containing secondary phases of Cu_2Se, In_2Se_3, etc.[9-20] This can be attributed to the major problems encountered due to the wide difference in the deposition potentials of Cu, In, and Se, which result in a deposit with a nonuniform composition.[16] Moreover, in the aqueous electrolyte used for electrodeposition of CIS, H^+ reduction causes composition inhomogeneity and hence limits the photovoltaic efficiency. For this reason, ionic liquids have also been studied for the deposition of CIS and CIGS films.[21,22] Besides, to overcome these problems, many researchers have used the annealing treatment in H_2Se or elemental Se atmosphere to get rid of unwanted phases. Along with being a highly toxic gas, selenization using H_2Se raises many problems, for example, inhomogeneity of the films after the selenization process due to an inhomogeneous Cu–In alloy layer, rapid volume expansion of CIS film during selenization [leading to poor adhesion of the films onto molybdenum back contacts], and phase separation of CIGS into CIS and $CuGaSe_2$.[23] Therefore, several different approaches were explored in order to overcome these issues. Recently, many researchers have used Cu–In alloy films with consequent selenization to get CIS films for photovoltaic application.[23-28] Here we would like to add another example to this list, where electrodeposited Se-coated Cu–In alloy was used as a precursor to obtain crystalline and single-phase CIS films.

In this paper we report on the electrochemical process of synthesizing crystalline CIS thin films from stacked layers of Cu–In alloy and Se, which are consecutively electrodeposited onto indium-tin-oxide (ITO) substrates and annealed at high temperatures to form CIS. The elemental selenium (Se) was deposited by the electrochemical route which provides a satisfactory deposition of elemental Se from aqueous electrolytes like H_2SeO_2, and these electrolytes are easy to handle and less toxic compared to H_2Se gas.

Experimental

For the deposition of Cu–In alloy thin films, aqueous solutions of [analytical reagent (AR) grade] 10 mM copper(II) sulfate ($CuSO_4$) and 10 mM indium(III) sulfate [$In_2(SO_4)_3$] complexed with aqueous H_2SO_4 (0.2 M) were combined together in equal proportion. For deposition of elemental Se thin films, aqueous solutions of (AR grade) 10 mM selenic(IV) acid (H_2SeO_3) were used. Electrodeposition of Cu–In alloy and Se thin films was carried out using a potentiostat (EG&G 273 A) in potentiostatic mode onto the ITO substrate. The substrate was thoroughly cleaned and subjected to ultrasonic treatment prior to deposition. A three-electrode cell configuration was formed from platinum plate as a counter electrode, the substrate was a working electrode placed vertically, and silver/silver chloride (Ag/AgCl) was the reference electrode (all the potentials are quoted with respect to Ag/AgCl). Prior to deposition, cyclic voltammetry (CV) curves at a scan rate of 20 mV/s were obtained in order to study the electrochemical changes as well as to determine the deposition potential. The preparative parameters were optimized to get adherent Cu–In alloy films onto the ITO substrates. The deposition of Cu–In films was carried out at applied constant potential −750 mV from the unstirred bath for different deposition periods. For deposition of the Se layer on formerly prepared Cu–In alloy film, a constant potential of −600 mV was applied under potentiostatic control for a period of 30 min from the unstirred bath. To convert Se-coated Cu–In films into CIS, the Se-coated Cu–In films were annealed at different temperatures in argon (Ar) atmosphere.

The Cu–In alloy, Se-coated Cu–In, and CIS films were characterized for their structural, and surface-morphological study. To study the structural property of the films, X-ray diffraction (XRD) patterns were obtained using an X-ray diffractometer (RINT/PMAX 2500, Rigaku, Japan) in the range of scanning angle 10–80° (2θ) with Cu Kα radiations. Surface morphological studies were carried out using scanning electron microscopy (SEM) images obtained with a field-emission SEM, (JSM-6340 F, Jeol, Japan).

Results and Discussion

CV.— CV is a powerful tool for the determination of formal redox potentials, detection of chemical reactions that precede or follow the electrochemical reaction, and evaluation of electron transfer kinetics.[29,30] During the scan, for any species that can be reduced through the range of potential scan, the current increases as

[z] E.mail: gujar_tp@yahoo.com; joocat@kist.re.kr

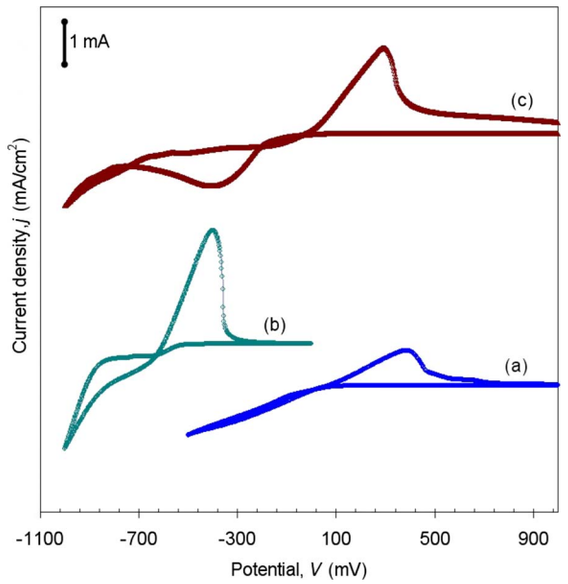

Figure 1. (Color online) CV curves obtained on ITO substrates from aqueous solutions of (a) $CuSO_4$, (b) $In_2(SO_4)_3$ and (c) a mixture of $CuSO_4$ + complexed $In_2(SO_4)_3$.

the potential reaches the reduction potential of the species. Thus, one can determine the reduction potential for a particular material to be deposited.

The CV curves in solutions of $CuSO_4$, $In_2(SO_4)_3$ complexed with dilute H_2SO_4, H_2SeO_3, and a mixture of Cu and In precursor solutions onto the ITO substrate at room temperature were used to monitor the electrochemical reactions as well as to find the suitable deposition potentials/currents range. All voltammetry curves were scanned first in the cathodic direction. Figure 1a shows the CV curve obtained individually from the solution of $CuSO_4$ on the ITO substrates. The voltammogram clearly depicts the well-defined cathodic (*Ec*) and anodic (*Ea*) peaks at −130 and +400 mV, respectively. The former peak corresponds to the deposition of copper metal and the latter to its dissolution. As discussed by Arenas et al.[31] the Cu^{2+} reduction occurs in a global step via two electrons, because the time for the existence of Cu^+ is short, not detectable by CV techniques, and can be considered to take place in the following manner

$$Cu^{2+}{}_{(aq)} + e^- \rightarrow Cu^+ \quad [1]$$

$$Cu^+ + e^- \rightarrow Cu_{(s)} \quad [2]$$

The voltammogram shows a crossover between cathodic current branches, which is a characteristic of the nucleation process.[32] Figure 1b shows CVs recorded from $In_2(SO_4)_3$ solution onto the ITO substrate. From $In_2(SO_4)_3$ solution complexed with dilute H_2SO_4, a reduction of In^{3+} occurred at a potential of −850 mV according to Reaction 3[33]

$$In^{3+}{}_{(aq)} + 3e^- \rightarrow In_{(s)} \quad [3]$$

The oxidation potential is seen at ca. −450 mV. The reduction potential of elemental In was shifted from standard potential to −850 mV (Fig. 1b). Here the complexation of $In_2(SO_4)_3$ with H_2SO_4 solution widens the deposition potential range of In. A cyclic voltammogram measured from a mixture of solutions of $CuSO_4$ and $In_2(SO_4)_3$ complexed with H_2SO_4 onto the ITO substrate at room temperature is shown in Fig. 1c. In this CV curve the first reduction point is observed at −230 mV, which corresponds to the reduction of elemental Cu. The deposition potential of Cu has been shifted compared with pure $CuSO_4$ solution (Fig. 1a). Similar shifts have been observed for Cu–Sn alloy deposition and have been attributed to the adsorption-site competition between the different precursors.[34,35] The deposition of Cu–In begins at a potential of −750 mV (Reactions 1-3). The steep rise in the cathodic current at a potential of −850 mV can be attributed to the onset of the formation of elemental In (cf. Fig. 1b). In the reversed scan the oxidation peak is observed at a potential of +470 mV, which is near that observed for a solution of $CuSO_4$, and thus it is most likely due to the oxidation of elemental Cu. Altogether, the above results lead to the conclusion that with these source concentrations stoichiometric Cu–In can be deposited between potentials of −750 and −800 mV.

A CV curve of a solution containing $HSeO_3^-$ on the ITO substrate, as explained in our previous report[36] (not shown here), exhibited the reduction point at a potential of −500 mV in forward CV scan due to the irreversible Reactions 4 and 5[37]

$$HSeO^-_{3(aq)} + 5H^+{}_{(aq)} + 4e^- \rightarrow Se_{(s)} + 3H_2O \quad [4]$$

$$Se_{(s)} + 2H^+{}_{(aq)} + 2e^- \rightarrow H_2Se_{(aq)} \quad [5]$$

The corresponding oxidation point, usually above +1000 mV,[37] is not seen here. The formation of elemental Se can be seen by holding the substrate at a constant overpotential of −500 mV and observing the appearance of a red Se deposit. In addition to Reactions 4 and 5, direct six-electron reduction of the $HSeO_3^-$ ion to H_2Se has also been reported.[38] The difference in reduction potential from earlier reports in the literature may be due to different substrates and other measurement conditions, such as stirring, pH, and concentration.[37,38] To deposit an Se layer on Cu–In alloy, an overpotential of −600 mV was applied for 30 min, and films were used as precursor for CIS films.

Further, the growth of Cu–In alloy onto ITO substrate and Se on Cu–In alloy was studied using chronoamperometry (CA), which is commonly used to study the mechanism of electrodeposition of metals and alloys with current transients. The CA curves during growth of Cu–In alloy and Se on Cu–In alloy are shown in Fig. 2a and b, respectively. Both transient curves exhibited an initial rapid increase in current with applied potential, further slowing current decay, followed by a nearly constant current. The observed rapid surge and exponential decay of the current are due to double-layer charge and immediately afterward the typical response of nucleation and growth by cluster formation, which is characteristic of diffusive controlled growth.[32,34] In the case of Cu–In alloy deposition, the current in the next region is slightly increased with time, which can be a consequence of low resistivity of Cu–In alloy. This graph indicates a progressive nucleation which corresponds to slow growth of nuclei on fewer active sites. For growth of Se on Cu–In alloy there is an increase in current, reaching its maximum, followed by a slow decrease; this is typical behavior for three-dimensional nucleation diffusion-limited growth. The CA graph for deposition of Se onto Cu–In alloy indicates an instantaneous nucleation which corresponds to fast growth of nuclei on many active sites, all activated during the course of electroreduction.

Investigations on Cu–In alloy.— Structural characterization of the Cu–In alloy film deposited onto ITO substrate was carried out using an XRD pattern within the 2θ range of 10–80°. Figure 3 shows the XRD patterns of (a) Cu–In alloy films onto the ITO substrates and (b) ITO glass substrate as a reference. The obtained patterns were compared with the standard International Center for Diffraction Data Powder Diffraction File (ICDD-PDF) Database (file no. 35-1150 and no. 41-0883) and the *d* values of CuIn and $Cu_{11}In_9$ are observed to be in good agreement with those reported in the standard PDF, possessing monoclinic structures. Along with diffraction peaks corresponding to ITO substrate, a series of characteristic peaks such as (101), (200), (102), ($\bar{1}$34), and (207) are identified for monoclinic CuIn phase, and ($11\bar{1}$), (312), and (511) are the peaks of the monoclinic $Cu_{11}In_9$ phase. No elemental In or Cu phases are observed. Volobujeva et al.[27] deposited CuIn alloy using magnetron sputtering of Cu/In alloy target, and they observed the

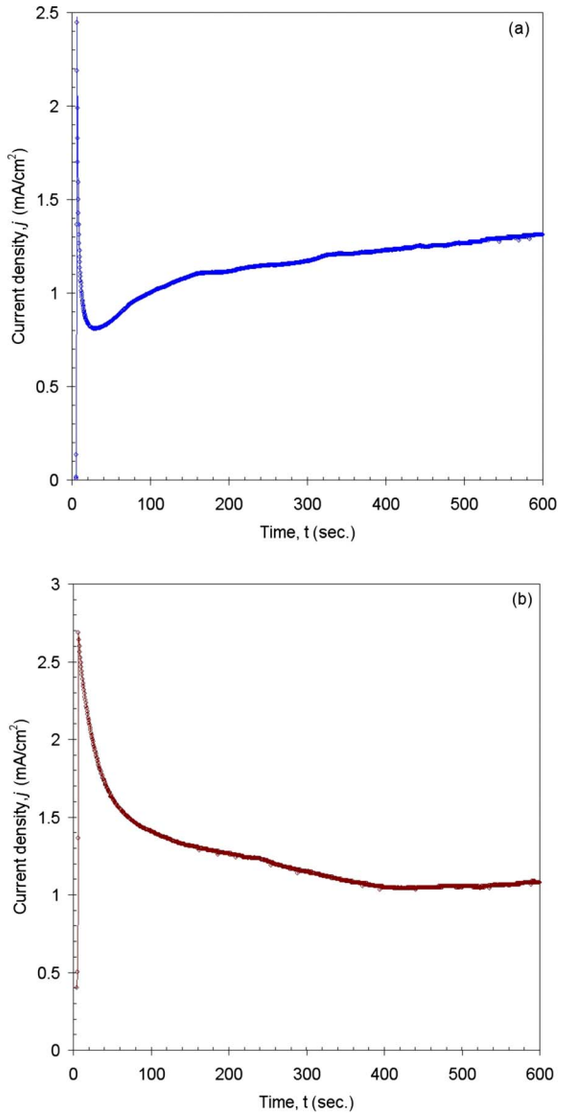

Figure 2. (Color online) Potentiostatic current–time transients recorded on (a) ITO electrode for Cu–In alloy and (b) Cu–In alloy for Se deposition.

$CuIn_2$ and $Cu_{11}In_9$ phases, while Luo et al.[28] deposited Cu–In alloy using pulsed laser deposition, and they observed the dominant $Cu_{11}In_9$ phase with secondary In phase. The formation of an elemental In or Cu phase may be disadvantageous, as this could lead to the formation of binary intermediate phases like InSe or CuSe by deposition of an Se layer.

The analysis of the surface morphology of the Cu–In alloy film was carried out by SEM. Figure 4 shows the typical morphologies of Cu–In alloy film was onto the ITO substrates. It can be clearly seen that along with the heaps of interconnected grains, the symmetrical dendritic structures have been grown. The central trunk consists of two orderly and regular rows of particles as shown in Fig. 4a and b. All the secondary branches consist of regular elongated particles, almost parallel to each other. As discussed earlier, due to the progressive growth, the new deposited Cu–In alloy particles may stick to any part of the formed clusters but are more likely to adhere to the tips of the cluster than to penetrate deep into its inner regions, leading to outward growth from the initial location of seed particles. Therefore, with an electrodeposition period, dendritic structures consisting of orderly and regular particles are formed.

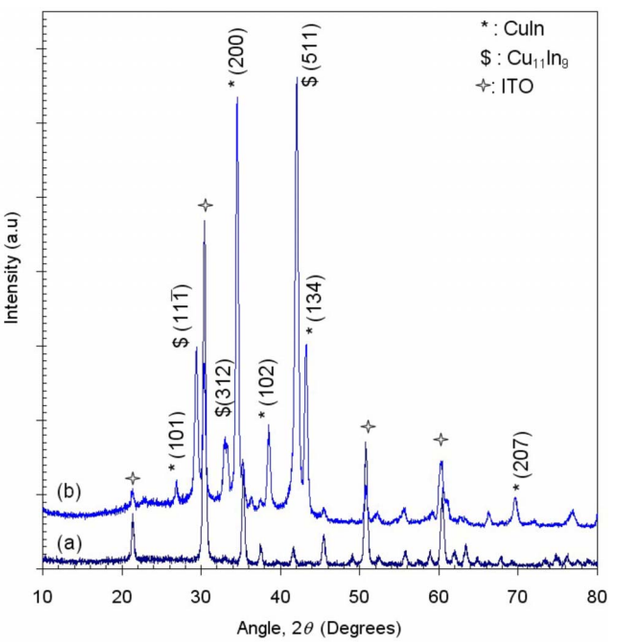

Figure 3. (Color online) XRD patterns of (a) Cu–In alloy film on the ITO substrates and (b) ITO glass substrate as a reference.

Investigations on Se-coated Cu–In alloy.— Cu–In alloy films are used as a substrate to deposit the elemental Se film. The XRD pattern of Se-coated Cu–In alloy is shown in Fig. 5a, and in Fig. 5b ITO glass substrate is shown as a reference. In this pattern, along with the peaks of Cu–In alloy and substrate peaks, the reflection peak corresponding to elemental Se is seen to be evolved at $2\theta = 22.96°$ (ICDD-PDF file no. 24-0714), which corresponds to monoclinic Se (deep red). Moreover, the XRD profile shows a background shape typical of an amorphous material, and it can be associated to the presence of amorphous selenium on Cu–In alloy.[36]

Se films synthesized onto the Cu–In alloy show interesting morphology, as is shown in Fig. 6. Figure 6a shows the low-magnification SEM micrograph of Se-coated Cu–In film, and it is seen that a deposit consists of elongated grains of nearly the same size. In Fig. 6b the higher magnification image indicates that the leaflike grains of Cu–In alloy are covered by an Se layer. These structures were used as a precursor for the CIS layer via thermal treatment to Se-coated Cu–In alloy.

Investigations on $CuInSe_2$ films.— Figure 7 shows the XRD patterns of (a) CIS film obtained from the Se-coated Cu–In alloy layer and (b) ITO glass substrate as a reference. From our experiments, optimal temperature and the time of thermal annealing of Se-coated

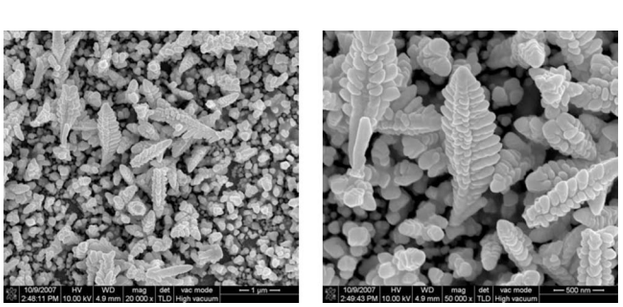

Figure 4. (a) Low- and (b) high-magnification SEM images of Cu–In alloy film on ITO substrates.

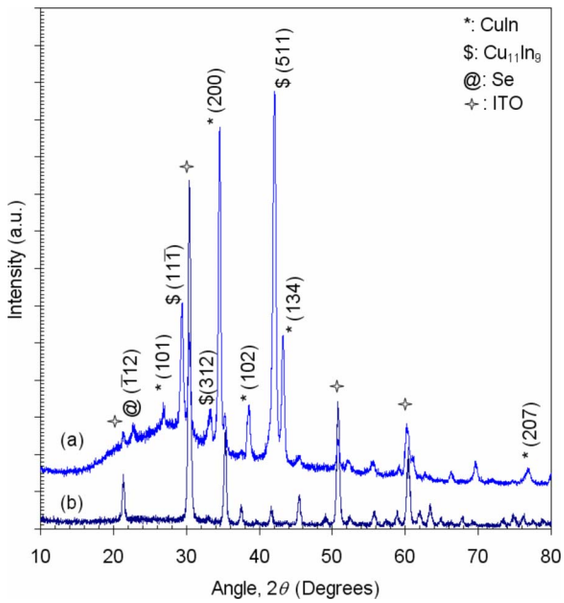

Figure 5. (Color online) XRD patterns of (a) Se-coated Cu–In alloy film and (b) ITO glass substrate as a reference.

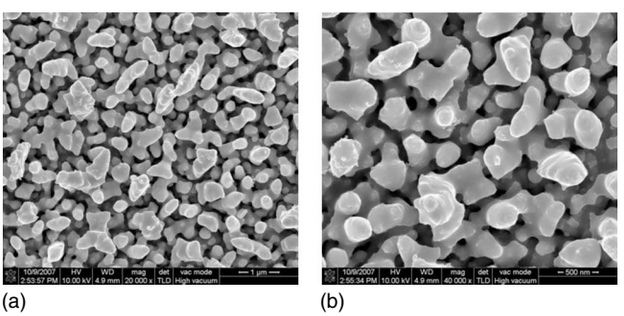

Figure 6. (a) Low- and (b) high-magnification SEM images of Se-coated Cu–In alloy film.

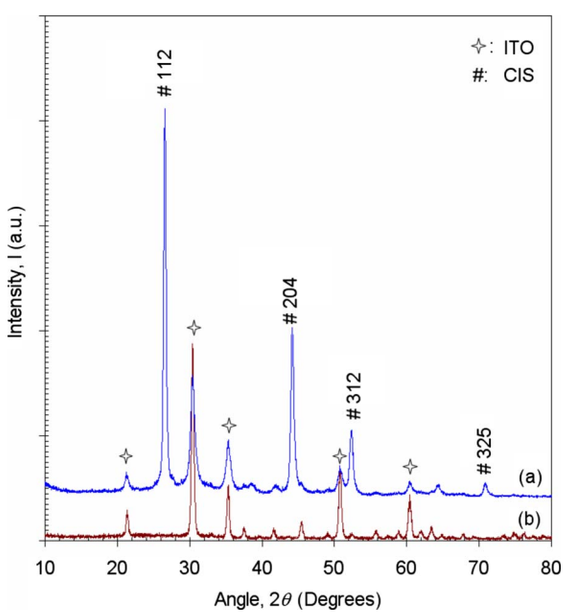

Figure 7. (Color online) XRD patterns of (a) $CuInSe_2$ film and (b) ITO glass substrate as a reference.

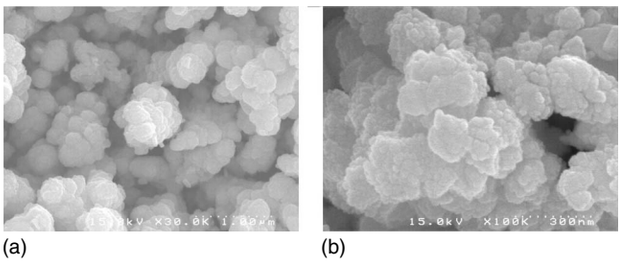

Figure 8. (a) Low- and (b) high-magnification SEM images of $CuInSe_2$ films.

Cu–In alloy precursor had been optimized at about 450°C for 30 min. The XRD pattern of the thermally annealed Se-coated Cu–In alloy was compared with the standard ICDD-PDF Database (file no. 40-1487), and the *d* values of the CIS obtained at all deposition potentials are observed to be in good agreement with those reported in the standard PDF, possessing chalcopyrite tetragonal structure (a = 5.782 and c = 11.619 Å). A series of characteristic peaks such as (112), (204), (312), and (325) are identified, and the intensities of these reflections are in agreement with the standard data from ICDD-PDF file no 40-1487. Secondary phases like Cu_2Se and In_2Se_3 or any elemental peaks were not observed in the XRD patterns of the CIS films; these were mostly encountered by researchers who deposited CIS films from the two-step process.

The analyses of the surface morphology of annealed films were carried out by SEM. Figure 8 shows the morphology of CIS onto the ITO substrates. Figures 8a and b show the lower- and higher-magnification SEM micrograph of a CIS film. It is seen that a deposit consists of a well-defined agglomerated multigrain structure with a size of ~450 nm. These grains are formed by incorporation of Se into Cu–In alloy.

Conclusions

Highly crystalline, single-phase CIS films were obtained by the electrochemical approach from Se-coated Cu–In alloy. The electrodeposited Cu–In alloy precursors showed the dominant CuIn phase and leaflike structures formed by interconnection between grains. The electrodeposition of an Se layer onto the Cu–In film gave total coverage on the surface. All the thermally treated Se-coated Cu–In alloy films at 450°C for 30 min gave CIS films with high orientation along the (112) plane of the chalcopyrite structure, and the agglomerated multigrain structure was formed on substrates. In this study, stoichiometry and good quality of CIS films were obtained by the electrodeposition method.

Acknowledgment

This work was supported by the Hydrogen Energy Research and Development Center, one of the 21st Century Frontier Research and Development programs, funded by the Ministry of Science and Technology of Korea.

Korea Institute of Science and Technology assisted in meeting the publication costs of this article.

References

1. I. Repins, M. A. Contreras, B. Egaas, C. DeHart, J. Scharf, C. L. Perkins, B. To, and R. Noufi, *Prog. Photovoltaics*, **16**, 235 (2008).
2. A. Ihlal, K. Bouabid, D. Soubane, M. Nya, O. A. T. Ali, Y. Amira, A. Outzourhit, and G. Nouet, *Thin Solid Films*, **515**, 5852 (2007).
3. S. H. Yoon, K. W. Seo, S. S. Lee, and W. Shim II, *Thin Solid Films*, **515**, 1544 (2006).
4. S. Niki, A. Yamada, R. Hunger, P. J. Fons, K. Iwata, K. Matsubara, A. Nishio, and H. Nakanishi, *J. Cryst. Growth*, **237–239**, 1993 (2002).
5. M. Dhanam, R. Balasundaraprabhu, S. Jayakumar, P. Gopalakrishnan, and M. D. Kannan, *Phys. Status Solidi A*, **191**, 149 (2002).
6. J. Yang, Z. Jin, T. Liu, C. Li, and Y. Shi, *Sol. Energy Mater. Sol. Cells*, **92**, 621 (2008).
7. D. Lincot, J. F. Guillemoles, S. Taunier, D. Guimard, J. S. Kurdi, A. Chaumont, O.

Roussel, O. Ramdani, C. Hubert, and J. P. Fauvarque, *Sol. Energy*, **77**, 725 (2004).
8. S. Bereznev, J. Kois, I. Golovtsov, A. Opik, and E. Mellikov, *Thin Solid Films*, **511–512**, 425 (2006).
9. J. Kois, S. Bereznev, O. Volobujeva, and E. Mellikov, *Thin Solid Films*, **515**, 5871 (2007).
10. S. Jost, F. Hergert, R. Hock, J. Schulze, A. Kirbs, T. Vox, and M. Purwins, *Sol. Energy Mater. Sol. Cells*, **91**, 1669 (2007).
11. S. Beyhan, S. Suzer, and F. Kadirgan, *Sol. Energy Mater. Sol. Cells*, **91**, 1922 (2007).
12. J. Araujo, R. Ortiz, A. Lopez-Rivera, J. M. Ortega, M. Montilla, and D. Larcon, *J. Solid State Electrochem.*, **11**, 407 (2007).
13. M. Valdes, M. A. Frontini, M. Vazquez, and A. Goossens, *Appl. Surf. Sci.*, **54**, 303 (2007).
14. S. M. Babu, A. Ennaoui, and M. C. Lux-Steiner, *J. Cryst. Growth*, **275**, e1241 (2005).
15. C. J. Huang, T. H. Meen, M. Y. Lai, and W. R. Chen, *Sol. Energy Mater. Sol. Cells*, **82**, 553 (2004).
16. M. C. F. Oliveira, M. Azevedo, and A. Cunha, *Thin Solid Films*, **405**, 129 (2002).
17. K. T. L. De Silva, W. A. A. Priyantha, J. K. D. S. Jayanetti, B. D. Chithrani, W. Siripal, K. Blake, and I. M. Dharmadasa, *Thin Solid Films*, **382**, 158 (2001).
18. F. Chraibi, M. Fahoume, A. Ennaoui, and J. L. Delplancke, *Phys. Status Solidi A*, **186**, 373 (2001).
19. A. Kampmann, P. Cowache, D. Lincot, and J. Vedel, *J. Electrochem. Soc.*, **146**, 150 (1999).
20. C. Guille, M. A. Martm, and J. Herrero, *Vacuum*, **58**, 594 (2000).
21. D. D. Shivagan, P. J. Dale, A. P. Samantilleke, and L. M. Peter, *Thin Solid Films*, **515**, 5899 (2007).
22. S. Z. El-Abedin, A. Y. Saad, H. K. Farag, N. Borisenko, Q. X. Liu, and F. Endres, *Electrochim. Acta*, **52**, 2746 (2007).
23. M. Sugiyama, F. B. Dejene, A. Kinoshita, M. Fukaya, Y. Maru, T. Nakagawa, H. Nakanishi, V. Alberts, and S. F. Chich, *J. Cryst. Growth*, **294**, 214 (2006).
24. F. O. Adurodija, J. Song, S. D. Kim, S. H. Kwon, S. K. Kim, K. H. Yoon, and B. T. Ahn, *Thin Solid Films*, **338**, 13 (1999).
25. S. D. Kim, H. J. Kim, K. H. Yoon, and J. Song, *Sol. Energy Mater. Sol. Cells*, **62**, 357 (2000).
26. T. Pisarkiewicz and H. Jankowski, *Vacuum*, **70**, 435 (2003).
27. O. Volobujeva, M. Altosaar, J. Raudoja, E. Mellikov, M. Grossberg, L. Kaupmees, and P. Barvinschi, *Sol. Energy Mater. Sol. Cells*, In press.
28. P. Luo, C. Zhu, and G. Jiang, *Solid State Commun.*, **146**, 57 (2008).
29. M. Noel and K. Vasu, *Cyclic Voltammetry and the Frontiers of Electrochemistry*, Aspect, London (1990).
30. V. S. Bagotsky, *Fundamentals of Electrochemistry*, John Wiley & Sons, New York (2005).
31. J. V. Arenas, G. Vazquez, A. M. Melendez, and I. Gonzalez, *J. Electrochem. Soc.*, **154**, D473 (2007).
32. S. B. Sadale and P. S. Patil, *Solid State Ionics*, **167**, 273 (2004).
33. M. Pourbaix, *Atlas of Electrochemical Equilibria*, Pergamon Press, New York (1966).
34. A. N. Correia, M. X. Facanha, and P. de L. Neto, *Surf. Coat. Technol.*, **201**, 7216 (2007).
35. C. Natarajan, M. Sharon, C. Levy-Clement, and M. N. Spallart, *Thin Solid Films*, **237**, 118 (1994).
36. T. P. Gujar, W. Y. Kim, K. D. Jung, and O. S. Joo, *J. Electrochem. Soc.*, **155**, E57 (2008).
37. H. Saloniemi, T. Kanniainen, M. Ritala, M. Leskela, and R. Lappalainen, *J. Mater. Chem.*, **8**, 651 (1998).
38. M. S. Kazacos and B. Miller, *J. Electrochem. Soc.*, **127**, 869 (1980).